

**Tribo-performance of polyester hybrid composites:
Damage assessment and parameter optimization using
Taguchi design**

[Materials & Design](#) 2008

<http://dx.doi.org/10.1016/j.matdes.2008.04.057>

Archived in Dspace@nitr

<http://dspace.nitrkl.ac.in/dspace>

Tribo-performance of polyester hybrid composites: Damage assessment and parameter optimization using Taguchi design

Amar Patnaik^{a,*}, Alok Satapathy^b, S.S. Mahapatra^b, R.R. Dash^c

^a Department of Mechanical Engineering, National Institute of Technology, Hamirpur 177 005, India

^b Department of Mechanical Engineering, National Institute of Technology, Rourkela 769 008, India

^c Department of Mechanical Engineering, G.I.E.T, Gunupur 765 022, India

A B S T R A C T

This paper investigates the solid particle erosion wear performance of a multi component hybrid composite consisting of polyester, glass fibers and alumina particles. A mathematical model for damage assessment in erosion is developed and validated by a well designed set of experiments. For this, the design of experiments approach using Taguchi's orthogonal arrays is used. The study reveals that glass-polyester composite without any filler suffers greater erosion loss than the hybrid composite with alumina filling. Significant control factors and their interactions that influence the wear rate are identified. Finally, optimal factor settings are determined using genetic algorithm.

1. Introduction

Composite material structures are synergistic combination of two or more micro-constituents that differ in physical form and chemical combination and which are insoluble in each other. The objective of having two or more constituents is to take advantage of the superior properties of both materials without compromising on the weakness of either. In a fiber reinforced composite, the fibers carry the bulk load and the matrix serves as the medium for the transfer of the load. Addition of filler materials further improves the functional properties of these composites. Such a multi-component composite system consisting of matrix, fiber and particulate filler is called a hybrid composite. Applications of such structures are observed in aircraft components, offshore and marine, industrial, military and defense, transportation, power generation etc. In these places, fiber reinforced polymers have to function in severe erosive environment and this often leads to their failure. Hard particulate fillers consisting of ceramic or metal particles and fiber fillers made of glass are being used these days to dramatically improve the wear resistance, even up to three orders of magnitude [1]. The improved performance of polymer composites in tribological applications by the addition of filler materials has shown a great promise and so has become a subject of considerable interest. The filler materials include organic, inorganic and metallic particulate materials in both micro and nano sizes. Various kinds of polymers and polymer matrix composites reinforced with metal particles have a wide range of industrial applications such as heat-

ers, electrodes [2], composites with thermal durability at high temperature [3] etc. These engineering composites are desired due to their low density, high corrosion resistance, ease of fabrication, and low cost [4-6]. Similarly, ceramic filled polymer composites have been the subject of extensive research in last two decades. The inclusion of inorganic fillers into polymers for commercial applications is primarily aimed at the cost reduction and stiffness improvement [7,8]. Along with fiber reinforced composites, the composites made with particulate fillers have been found to perform well in tribological conditions. Such composites are called hybrid composites.

Erosive wear of engineering components caused by abrasive particles is a major industrial problem. A full understanding of the effects of all system variables on the wear rate is necessary in order to undertake appropriate steps in the design of machine or structural component and in the choice of materials to reduce/control wear. In recent years much research has been devoted to exploring the potential advantages of thermoplastic polymers for composite materials. Some of the commonly used thermoplastics are polyetheretherketone (PEEK), polyetherketone (PEK), polyetherketoneketone (PEKK), polyester, polypropylene (PP) etc. Several investigations on friction and wear properties of PEEK and its composites filled with fibers, organic and inorganic fillers have been carried out [9,18]. Cirino et al. [9,10] reported the sliding as well as the abrasive wear behaviour of continuous carbon and aramid fiber reinforced PEEK. Lhymn et al. [11] have studied the abrasive wear of short carbon fibre reinforced PEEK. Voss and Friedrich [12] investigated the sliding and abrasive wear behavior of short fiber reinforced PEEK composites at room temperature. While Briscoe et al. [13] described the friction and wear of PEEK-PTFE

Nomenclature

R	chord length of the indentation (m)	m	mass of single erodent particle (kg)
d	erodent diameter (m)	M	mass flow rate of the erodent (kg/s)
δ	indentation depth (m)	N	number of impact per unit time (s^{-1})
e_v	volumetric wear loss per particle impact (m^3)	ρ_c	density of composite (kg/m^3)
E_v	total volumetric erosion wear rate (m^3/s)	ρ	density of erodent (kg/m^3)
α	angle of impingement (degree)	η_{normal}	erosion efficiency with normal impact
V	impact velocity (m/s)	η	erosion efficiency
P	force on the indenter (N)	E_{rth}	erosion wear rate (kg/kg)
H_v	hardness (N/m^2)		

blends over a wide composition range under several testing conditions, Friedrich et al. [14] reported an extensive overview on polymer composites for friction and wear application. Bahadur and Gong [15] investigated the action of various copper compounds as fillers on the tribological behaviour of PEEK. Wang et al. [16–18] investigated friction and wear properties of nanometric ZrO_2 and SiC filled PEEK composites with different filler proportions. Most of the above studies are confined to dry sliding wear of PEEK and its composites. The erosive wear behavior of polyester composites reinforced with any fiber or particulate matter has not yet been reported in the literature. In view of the above, the objective of the present investigation is to study the effect of glass fiber reinforcement and inclusion of alumina filler on the erosive wear behavior of polyester under multiple impact conditions.

Aluminum oxide (Al_2O_3) commonly referred to as ‘alumina’ is the most cost effective and widely used material in the family of engineering ceramics. It also has the potential to be used as filler material in various polymer matrices. Alumina can exist in several crystalline phases which all revert to the most stable hexagonal alpha phase at elevated temperatures. This is the phase of particular interest for structural applications. Al_2O_3 is hard, wear-resistant, has excellent dielectric properties, resistance to strong acid and alkali attack at elevated temperatures, high strength and stiffness. With an excellent combination of properties and a reasonable price, it is no surprise that fine grain technical grade alumina has a very wide range of applications.

To obtain the desired properties from a hybrid composite system, reinforcement and fillers are added to the polymers. The additional improvements in mechanical and tribological properties are in many cases attained through the incorporation of glass or carbon fiber reinforcement and through the filling of particulate matters. However, tribo-properties are not intrinsic material properties, but strongly depend upon the system in which material functions [19]. So the influence of fillers and fibers on the tribo-behavior of composites cannot be predicted a priori and has to be tested in the laboratory. In many industrial applications of composites, an understanding of tribological behavior is also necessary along with an understanding of the mechanical properties [20]. Hence, the primary concern here is to study how the alumina particle filled glass fiber reinforced polyester composites respond to the impact of erodent under different operating conditions, to assess the damage due to wear and finally to determine the optimal parameter settings for minimum wear loss.

2. Mathematical model

Solid particle erosion is a wear process in which the material is removed from a surface by the action of a stream of erodent particles entrained in a high velocity fluid stream. The particles strike against the surface and promote material loss. During flight, a particle carries momentum and kinetic energy which can be dissipated during the impact due to its interaction with a target surface. As far

as erosion study of polymer matrix composites is concerned, no specific model has been developed and thus the study of their erosion behavior has been mostly experimental. However, Mishra [21] proposed a mathematical model for material removal rate in abrasive jet machining process in which the material is removed from the work piece in a similar fashion. This model assumes that the volume of material removed is same as the volume of indentation caused by the impact. This has a serious limitation as in a real erosion process the volume of material removed is actually different from the indentation volume. Further, this model considers only the normal impact i.e. $\alpha = 90^\circ$ whereas in actual practice, particles may impinge on the surface at any angle ($0^\circ \leq \alpha \leq 90^\circ$). The proposed model addresses these shortcomings in an effective manner. It considers the real situation in which the volume of material removed by erosion is not same as the volume of material displaced and therefore, an additional term ‘erosion efficiency (η)’ is incorporated in the erosion wear rate formulation. In case of a stream of particles impacting a surface normally (i.e. at $\alpha = 90^\circ$), erosion efficiency (η_{normal}) defined by Sundararajan et al. [22] is given as

$$\eta_{normal} = \frac{2E_r H_v}{\rho V^2} \quad (1)$$

But considering impact of erodent at any angle α to the surface, the actual erosion efficiency can be obtained by modifying Eq. (1) as

$$\eta = \frac{2E_r H_v}{\rho V^2 \sin^2 \alpha} \quad (2)$$

The model is based on the assumption that the kinetic energy of the impinging particles is utilized to cause micro-indentation in the composite material and the material loss is a measure of the indentation. The erosion is the result of cumulative damage of such non-interacting, single particle impacts. The model further assumes the erodent particles to be rigid, spherical bodies of diameter equal to the average grit size. It considers the ductile mode of erosion and assumes that the volume of material lost in a single impact is less than the volume of indentation. The model is

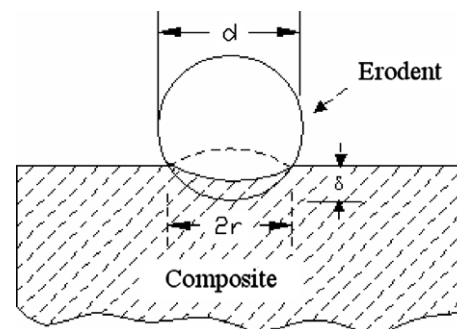


Fig. 1. Scheme of material removal mechanism in ductile mode.

developed with the simplified approach of energy conservation which equates the erodent kinetic energy with the work done in creating the indentation.

The model for ductile mode erosion proceeds as follows.

From the geometry of Fig. 1, $r^2 = d \times \delta$

The volume of indentation = $\pi \delta^2 \left[\frac{d}{2} - \frac{\delta}{3} \right]$

So, the volumetric wear loss per particle impact is given by

$$\begin{aligned} e_v &= \text{Volume of indentation} \times \eta \\ &= \eta \times \pi \delta^2 \left[\frac{d}{2} - \frac{\delta}{3} \right] \text{ and neglecting } \delta^3 \delta \text{ terms} \\ &= \frac{\pi \cdot d \cdot \delta^2}{2} \times \eta \end{aligned}$$

Considering N number of particle impacts per unit time, the volumetric erosion wear loss will be

$$E_v = \frac{\pi \cdot d \cdot \delta^2}{2} N \times \eta \quad (3)$$

The impact velocity will have two components; one normal to the composite surface and one parallel to it. At zero impact angles, it is assumed that there is negligible wear because eroding particles do not practically impact the target surface [23]. Consequently, there will be no erosion due to the parallel component and the indentation is assumed to be caused entirely by the component normal to the composite surface as shown in Fig. 2.

Now applying conservation of energy to the single impact erosion process, kinetic energy associated with the normal velocity component of a single erodent particle is equal to the work done in the indentation of composite. The energy of impact introduces a force P on the indenter to cause the indentation in the composite. Thus

$$\frac{1}{2} m v^2 \sin^2 \alpha = \frac{1}{2} \cdot P \cdot \delta \quad (4)$$

$$\text{So, } \frac{1}{2} \left(\frac{\pi d^3}{6} \right) \rho v^2 \sin^2 \alpha = \frac{1}{2} (\pi r^2 H) \delta$$

$$\text{On solving; } \delta^2 = \frac{\rho \cdot V^2 d^2 \sin^2 \alpha}{6H} \quad (5)$$

The number of erodent particle impacting the target is estimated from the known value of erodent mass flow rate, M as

$$N = \frac{M}{\frac{\pi d^3}{6} \rho} \quad (6)$$

Substituting the value of δ in Eq. (3)

$$E_v = \frac{\pi \cdot d \cdot d^2 \cdot V^2 \cdot \sin^2 \alpha \cdot \rho}{2 \times 6H} \cdot \frac{M \cdot 6}{\pi \cdot d^3 \rho} \cdot \eta$$

$$E_v = \frac{V^2 \cdot \sin^2 \alpha}{2H} \cdot \eta \cdot M$$

Erosion rate (E_r) defined as the ratio of mass lost due to erosion to the mass of erodent is now expressed as

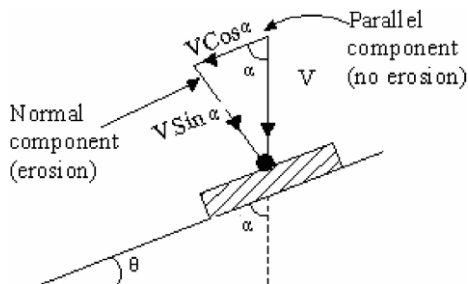


Fig. 2. Resolution of impact velocity in normal and parallel directions.

$$E_{\text{erth}} = \frac{\rho_c \cdot \eta \cdot V^2 \cdot \sin^2 \alpha}{2H} \quad (7)$$

Material removal by impact erosion wear involves complex mechanisms. A simplified theoretical model for such a process may appear inadequate unless its assessment against experimental results is made. So for the validation of the proposed model, erosion tests on the composites are conducted at various operating conditions.

3. Experimental details

3.1. Specimen preparation

E-glass fibers (360 roving taken from Saint Govion) are reinforced in alumina filled unsaturated isophthalic polyester resin to prepare hybrid composites. The composite slabs are prepared by conventional hand-lay-up technique. Two percentage of cobalt naphthalate (as accelerator) is mixed thoroughly in isophthalic polyester resin and then 2% methyl-ethyl-ketone-peroxide (MEKP) as hardener is mixed in the resin prior to reinforcement. The filler material alumina (average size 50 μm , density 3.89 gm/cc) is provided by NICE Ltd India. E-glass fiber and polyester resin have modulus of 72.5 GPa and 3.25 GPa, respectively and possess density of 2590 kg/m³ and 1350 kg/m³, respectively. Composites of three different compositions (0 wt%, 10 wt% and 20 wt% alumina filling) are made and the fiber loading (weight fraction of glass fiber in the composite) is kept at 50% for all the samples. The castings are put under load for about 24 h for proper curing at room temperature. Specimens of suitable dimension are cut using a diamond cutter for physical characterization and erosion test.

3.2. Test apparatus

Fig. 3 shows the schematic diagram of erosion test rig conforming to ASTM G 76. The set up is capable of creating reproducible erosive situations for assessing erosion wear resistance of the prepared composite samples. It consists of an air compressor, an air particle mixing chamber and accelerating chamber. Dry compressed air is mixed with the particles which are fed at constant rate from a sand flow control knob through the nozzle tube and then accelerated by passing the mixture through a convergent brass nozzle of 3 mm internal diameter. These particles impact the specimen which can be held at different angles with respect to the direction of erodent flow using a swivel and an adjustable sample clip. The velocity of the eroding particles is determined using standard double disc method [24]. In the present study, dry silica sand (spherical) of different particle sizes (300 μm , 500 μm and 800 μm) are used as erodent. The samples are cleaned in acetone, dried and weighed to an accuracy of ± 0.1 mg before and after the erosion trials using a precision electronic balance. The weight loss is recorded for subsequent calculation of erosion rate. The process is repeated till the erosion rate attains a constant value called steady state erosion rate.

3.3. Test of micro-hardness, density, tensile and flexural properties

Micro-hardness measurement is done using a Leitz micro-hardness tester. A diamond indenter, in the form of a right pyramid with a square base and an angle 136° between opposite faces, is forced into the material under a load F . The two diagonals X and Y of the indentation left on the surface of the material after removal of the load are measured and their arithmetic mean L is calculated. In the present study, the load considered $F = 24.54\text{N}$ and Vickers hardness number is calculated using the following equation

$$H_v = 0.1889 \frac{F}{L^2} \quad (8)$$

and

$$L = \frac{X + Y}{2}$$

where F is the applied load (N), L is the diagonal of square impression (mm), X is the horizontal length (mm) and Y is the vertical length (mm).

The tensile test is generally performed on flat specimens. The commonly used specimen for tensile test is the dog-bone specimen and straight side specimen with end tabs. A uniaxial load is applied through both the ends. The ASTM standard test method for tensile properties of fiber resin composites has the designation D 3039-76. The length of the test section should be 200 mm. The tensile test is performed in the universal testing machine Instron 1195 and results are analyzed to calculate the tensile strength of composite samples.

The flexural strength of a composite is the maximum tensile stress that it can withstand during bending before reaching the breaking point. The three point bend test is conducted on all the composite samples in the universal testing machine Instron 1195. Span length of 40 mm and the cross head speed of 10 mm/min are maintained.

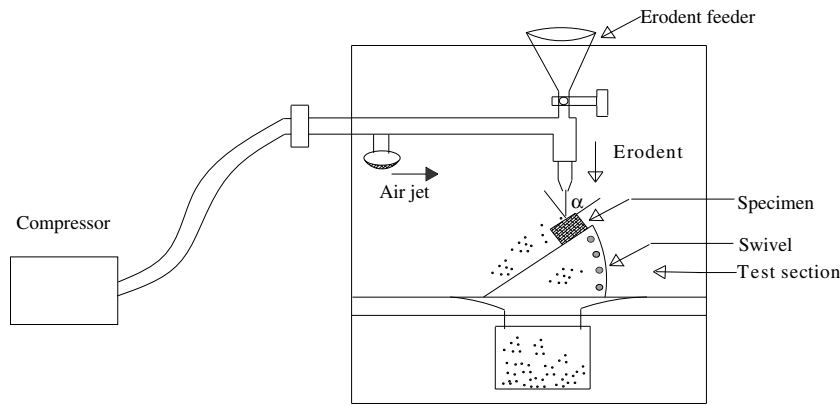


Fig. 3. A schematic diagram of the erosion test rig.

The surfaces of the specimens are examined directly by scanning electron microscope JEOL JSM-6480LV. The eroded samples are mounted on stubs with silver past. To enhance the conductivity of the eroded samples, a thin film of platinum is vacuum-evaporated onto them before the photomicrographs are taken.

3.4. Experimental design

Design of experiment is a powerful analysis tool for modeling and analyzing the influence of control factors on performance output. The most important stage in the design of experiment lies in the selection of the control factors. Therefore, a large number of factors are included so that non-significant variables can be identified at earliest opportunity. Exhaustive literature review on erosion behavior of polymer composites reveal that parameters viz., impact velocity, impingement angle, fiber loading, filler content, erodent size and stand-off distance etc largely influence the erosion rate of polymer composites [25,26]. The impact of five such parameters are studied using $L_{27} (3^{13})$ orthogonal design. The operating conditions under which erosion tests are carried out are given in Table 1. The tests are conducted as per experimental design given in Table 2 at room temperature.

In Table 2, each column represents a test parameter whereas a row stands for a treatment or test condition which is nothing but combination of parameter levels. In conventional full factorial experiment design, it would require $3^5 = 243$ runs to study five parameters each at three levels whereas, Taguchi's factorial experiment approach reduces it to only 27 runs offering a great advantage in terms of experimental time and cost. The experimental observations are further transformed into signal-to-noise (S/N) ratio. There are several S/N ratios available depending on the type of performance characteristics. The S/N ratio for minimum erosion rate can be expressed as "lower is better" characteristic, which is calculated as logarithmic transformation of loss function as shown below

$$\text{Smaller is the better characteristic : } \frac{S}{N} = -10 \log_{10} \left(\frac{1}{n} \sum y^2 \right) \quad (9)$$

where 'n' the number of observations, and y the observed data. The standard linear graph, as shown in Fig. 4, is used to assign the factors and interactions to various columns of the orthogonal array [27].

The plan of the experiments is as follows: the first column is assigned to impact velocity (A), the second column to alumina percentage (B), the fifth column to stand-off distance (C), the ninth column to impingement angle (D) and the tenth column to erodent size (E), the third and fourth column are assigned to $(A \times B)_1$ and $(A \times B)_2$, respectively to estimate interaction between impact velocity (A) and alumina percentage (B), the eighth and eleventh column are assigned to $(A \times C)_1$ and $(A \times C)_2$, respectively to estimate interaction between the impact velocity (A) and stand-off distance (C) and the remaining columns are used to estimate experimental errors.

Table 1
Levels of the variables used in the experiment

Control factor	Level			Units
	I	II	III	
A: Velocity of impact	32	45	58	m/s
B: Alumina percentage	0	10	20	%
C: Stand off distance	120	180	240	mm
D: Impingement angle	45	60	90	deg.
E: Eroder size	300	500	800	μm

4. Results and discussion

4.1. Mechanical properties

In the present investigation the addition of alumina filler in glass polyester hybrid composite has not shown encouraging results in terms of mechanical properties. Figs. 5a and 5b present the tensile strengths and tensile moduli of the composites with and without filler. It can be seen that the tensile properties have become distinctly poorer with the incorporation of alumina particles in the matrix. Previous reports [28,29] demonstrate that normally the glass fibers in the composite restrain the deformation of the matrix polymer reducing the tensile strain. So even if the strength decreases with filler addition the tensile modulus of the hybrid composite is expected to increase. But this is possibly not occurring in the present case with the presence of alumina as the filler and as a result reduction in both tensile strength and modulus is recorded in spite of the reinforcement of long glass fibers. Moreover, alumina affecting the crystalline structure of semi-crystalline thermoplastic polyester may also be another reason for the deterioration of tensile properties. This might have influenced the flexural strength of these hybrid composites which is showing (Fig. 6) a decreasing trend beyond a filler content of 10 wt%.

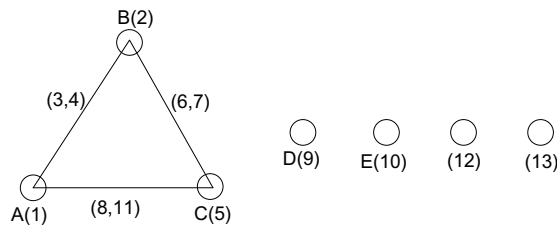
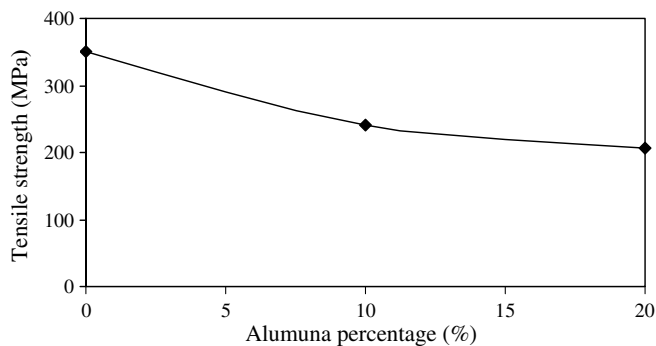
The micro-hardness of the glass polyester composite is not seen to have significantly changed with the addition of alumina (Fig. 7). However the density of the composites has reduced with alumina filling. The neat polyester taken for this study possess a density of 1.35 gm/cc which increases to 1.93 gm/cc with the reinforcement of 50 wt% of glass fiber in it. But when the matrix is filled with micro sized alumina particles the density of the resulting hybrid composite reduces and this reduction is almost proportional to the filler content (Fig. 8).

4.2. Surface morphology

Fig. 9a shows a portion of the composite surface before erosion occurred. Scattered alumina particles are observed on the upper surface. The distribution of filler as seen in the micrograph is reasonably uniform although at places the particles are seen to have formed small and big clusters. Fig. 9b shows the micrograph of surface eroded at an impingement angle of 60° and an impact velocity of 45 m/s. A small portion of a fiber exposed during the sand erosion is noticed. The matrix covering the fiber seems to be chipped off and the crater thus formed shows the fiber body which is almost intact. Repeated impact of the erodent has caused roughening of the surface. Erosion along the fibers and clean removal of the matrix at the interface is observed in the magnified image given alongside. Fig. 9c clearly shows the crater formation due to

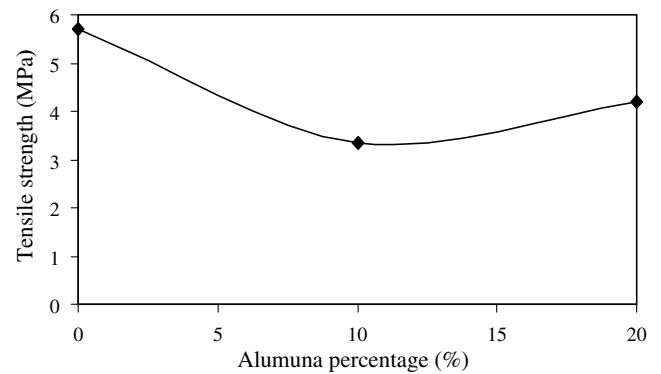
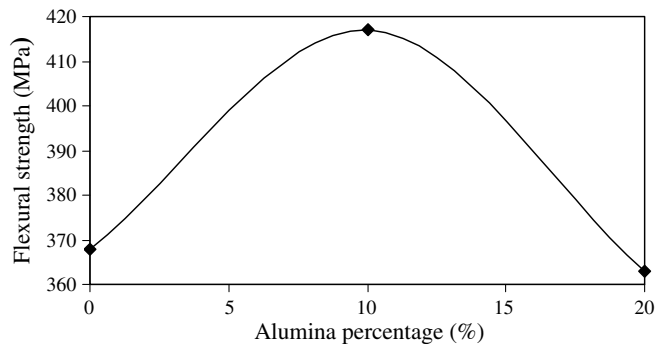
Table 2Orthogonal array for $L_{27}(3^{13})$ Taguchi design

$L_{27}(3^{13})$	1 A	2 B	3 ($A \times B$) ₁	4 ($A \times B$) ₂	5 C	6	7	8 ($A \times C$) ₁	9 D	10 E	11 ($A \times C$) ₂	12	13
1	1	1	1	1	1	1	1	1	1	1	1	1	1
2	1	1	1	1	2	2	2	2	2	2	2	2	2
3	1	1	1	1	3	3	3	3	3	3	3	3	3
4	1	2	2	2	1	1	1	2	2	2	3	3	3
5	1	2	2	2	2	2	2	3	3	3	1	1	1
6	1	2	2	2	3	3	3	1	1	1	2	2	2
7	1	3	3	3	1	1	1	3	3	3	2	2	2
8	1	3	3	3	2	2	2	1	1	1	3	3	3
9	1	3	3	3	3	3	3	2	2	2	1	1	1
10	2	1	2	3	1	2	3	1	2	3	1	2	3
11	2	1	2	3	2	3	1	2	3	1	2	3	1
12	2	1	2	3	3	1	2	3	1	2	3	1	2
13	2	2	3	1	1	2	3	2	3	1	3	1	2
14	2	2	3	1	2	3	1	3	1	2	1	2	3
15	2	2	3	1	3	1	2	1	2	3	2	3	1
16	2	3	1	2	1	2	3	3	1	2	2	3	1
17	2	3	1	2	2	3	1	1	2	3	3	1	2
18	2	3	1	2	3	1	2	2	3	1	1	2	3
19	3	1	3	2	1	3	2	1	3	2	1	3	2
20	3	1	3	2	2	1	3	2	1	3	2	1	3
21	3	1	3	2	3	2	1	3	2	1	3	2	1
22	3	2	1	3	1	3	2	2	1	3	3	2	1
23	3	2	1	3	2	1	3	3	2	1	1	3	2
24	3	2	1	3	3	2	1	1	3	2	2	1	3
25	3	3	2	1	1	3	2	3	2	1	2	1	3
26	3	3	2	1	2	1	3	1	3	2	3	2	1
27	3	3	2	1	3	2	1	2	1	3	1	3	2

**Fig. 4.** Linear graphs for L_{27} array.**Fig. 5a.** Effect of alumina filling on tensile strength of the hybrid composite.

penetration of hard silica sand particles onto the surface and cause material removal mostly from the matrix regime. Small cracks and multiple fractures are also distinctly shown in this micrograph.

Particle impingement produces a rise in temperature of the surface which makes the matrix deformation easy because the high temperature known to occur in solid particle erosion invariably soften the matrix [30]. On impact the erodent particle kinetic energy is transferred to the composite body that leads to crater formation and subsequently material loss. The presence of hard alumina particle in the matrix helps in absorbing a good fraction

**Fig. 5b.** Effect of alumina filling on tensile modulus of the hybrid composite.**Fig. 6.** Effect of alumina filling on flexural strength of the hybrid composites.

of this kinetic energy and therefore energy available for the plastic deformation of thermoplastic polyester becomes less. This also delays the initiation of fiber exposure as compared to the composite without any filler. All these factors combined together result in exhibition of better erosion response by the alumina filled

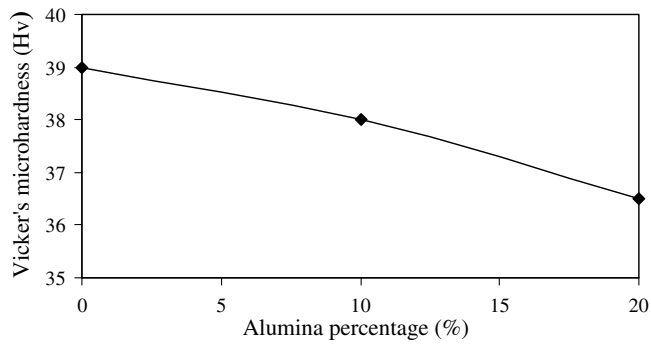


Fig. 7. Variation of Vicker's microhardness with alumina percentage.

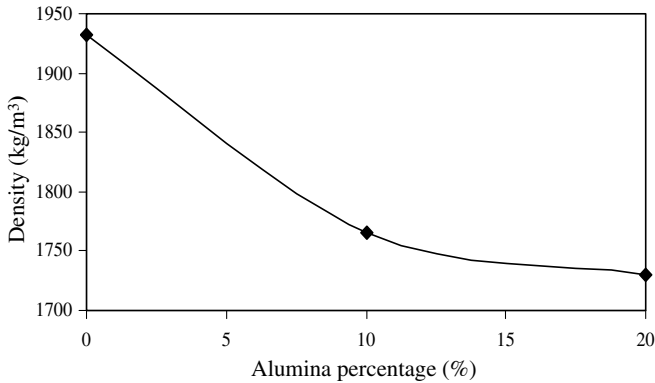


Fig. 8. Effect of alumina filling on density of the hybrid composite.

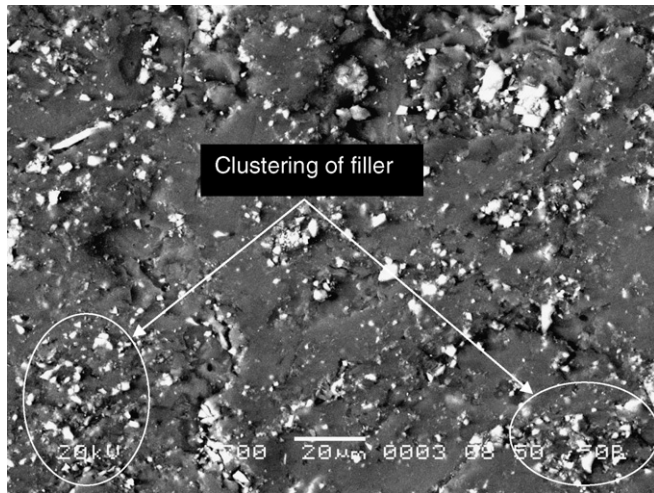


Fig. 9a. Scanning electron micrograph of uneroded composite surface (Alumina content 20%).

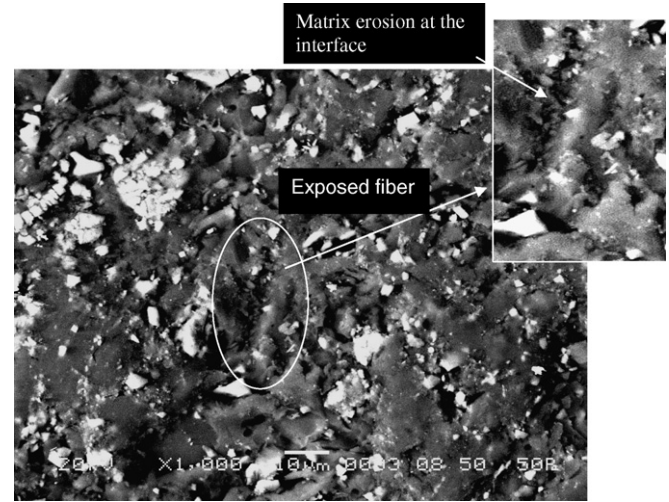


Fig. 9b. Scanning electron micrograph of eroded composite surface (impact velocity 45 m/s, alumina content 20%, S.O.D 180 mm, impingement angle 60° and erodent size 800 µm).

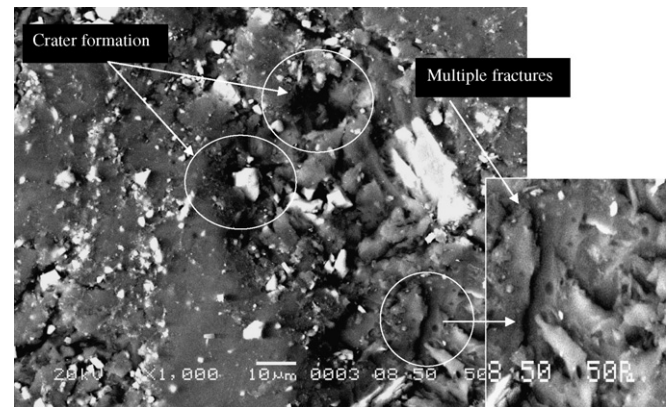


Fig. 9c. Scanning electron micrograph of eroded composite surface (impact velocity 58 m/s, alumina content 20%, S.O.D 180 mm, impingement angle 60° and erodent size 800 µm).

composites than that of fiber reinforced polyester without particulate filling.

4.3. Steady state erosion

Thermoplastic matrix composites usually show ductile erosion while the thermosetting ones erode in a brittle manner. Thus the erosion wear behavior of polymer composites can be grouped into ductile and brittle categories although this grouping is not definitive because the erosion characteristics equally depend on the experimental conditions as on composition of the target material.

It is well known that impingement angle is one of the most important parameters in the erosion process and for ductile materials the peak erosion occurs at 15° to 20° angle while for brittle materials the erosion damage is maximum usually at normal impact i.e. 90° angle. In the present study the variation of erosion wear rate of the hybrid composites with impingement angle under similar operating conditions is investigated. The result is presented in Fig. 10 which shows the peak erosion taking place at an impact angle of 60°. This clearly indicates that these hybrid composites respond to solid particle erosion in neither a purely ductile nor a purely brittle manner. This behavior can be termed as semi-ductile in nature. The loss of ductility may be attributed to the incorporation of glass fibers and alumina particles both of which are brittle.

In Table 3, the last column represents *S/N* ratio of the erosion rate which is in fact the average of two replications. The overall mean for the *S/N* ratio of the erosion rate is found to be -46.33 db. The analysis was made using the popular software specifically used for design of experiment applications known as MINITAB 14. Before any attempt is made to use this simple model as a predictor for the measure of performance, the possible interactions between the control factors must be considered. Thus factorial design incorporates a simple means of testing for the presence of the interaction effects.

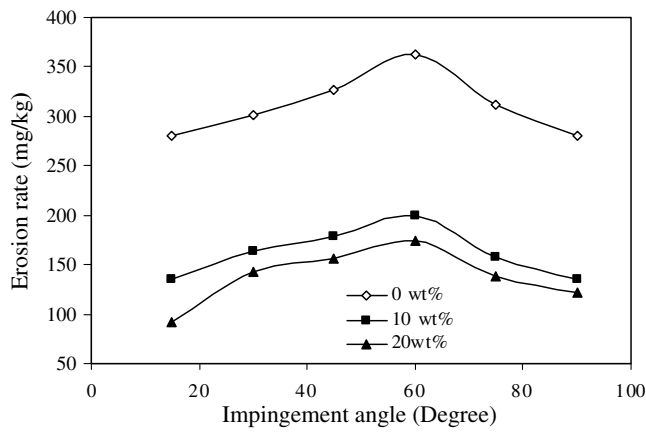


Fig. 10. Erosion rate vs. Angle of impingement for different alumina filling.

Analysis of the result leads to the conclusion that factor combination of A_1 , B_2 , C_3 , D_1 and E_2 gives minimum erosion rate. This is evident from Fig. 11. As far as minimization of erosion rate is concerned, factors A , B , D and E have significant effect whereas factor C has least effect. It is observed from Fig. 12 that the interaction between $A \times B$ shows most significant effect on erosion rate. From this analysis we concluded that few of the factors have individual effect on the erosion rate and similarly, few of the interactions have combined effect on erosion rate.

4.4. Erosion efficiency

The hardness alone is unable to provide sufficient correlation with erosion rate, largely because it determines only the volume displaced by each impact and not really the volume eroded. Thus a parameter which will reflect the efficiency with which the volume that is displaced is removed should be combined with hardness to obtain a better correlation. The erosion efficiency is

obviously one such parameter. This thought has already been reflected in the theoretical model but the evaluation of erosion efficiency can be made only on the basis of experimental data. Hence, the values of erosion efficiencies of these composites calculated using Eq. (2) are summarized in Table 4 along with their hardness values and operating conditions. It clearly shows that erosion efficiency is not exclusively a material property; but also depends on other operational variables such as impingement angle and impact velocity. The erosion efficiencies of these composites under normal impact (η_{normal}) vary from 3% to 6%, 6–9% and 9–12% for impact velocities 58 m/s, 45 m/s and 32 m/s, respectively. The value of η for a particular impact velocity under oblique impact can be obtained simply by multiplying a factor $1/\sin^2\alpha$ with η_{normal} . Similar observation on velocity dependence of erosion efficiency has previously been reported by few investigators [21,22].

The theoretical erosion wear rate (E_{rth}) of the alumina filled polyester-GF composites are calculated using Eq. (7). These values are compared with those obtained from experiments (E_{rexp}) conducted under similar operating conditions. Table 5 presents a comparison among the theoretical and experimental results. The corresponding comparison plot is shown in Fig. 13. The errors in experimental results with respect to the theoretical ones lie in the range 0–10%. The magnitude of η can be used to characterize the nature and mechanism of erosion. For example, ideal micro-ploughing involving just the displacement of the material from the crater without any fracture (and hence no erosion) will result in $\eta = 0$. In contrast, if the material removal is by ideal micro-cutting, $\eta = 1.0$ or 100%. If erosion occurs by lip or platelet formation and their fracture by repeated impact, as is usually the case in the case of ductile materials, the magnitude of η will be very low, i.e. $\eta \leq 100\%$. In the case of brittle materials, erosion occurs usually by spalling and removal of large chunks of materials resulting from the interlinking of lateral or radial cracks and thus η can be expected to be even greater than 100% [26]. The erosion efficiencies of the composites under the present study indicate that at low impact speed the erosion response is semi-ductile ($\eta = 10\text{--}100\%$). On

Table 3
Experimental design using L_{27} orthogonal array

Expt. no.	Impact velocity (A) m/s	Alumina percentage (B)%	Stand-off distance (C) mm	Impingement angle (D) degree	Erodent size (E) μm	Erosion rate (E_r) mg/kg	S/N ratio (db)
1	32	0	120	30	300	309.83	-49.8225
2	32	0	180	60	500	235.25	-47.4306
3	32	0	240	90	800	315.19	-49.9714
4	32	10	120	60	500	173.77	-44.7995
5	32	10	180	90	800	264.94	-48.4630
6	32	10	240	30	300	139.96	-42.9201
7	32	20	120	90	800	289.48	-49.2324
8	32	20	180	30	300	227.49	-47.1392
9	32	20	240	60	500	197.88	-45.9280
10	45	0	120	60	800	318.86	-50.0720
11	45	0	180	90	300	349.80	-50.8764
12	45	0	240	30	500	235.25	-47.4306
13	45	10	120	90	300	174.94	-44.8578
14	45	10	180	30	500	133.18	-42.4888
15	45	10	240	60	800	172.78	-44.7499
16	45	20	120	30	500	183.96	-45.2945
17	45	20	180	60	800	287.83	-49.1827
18	45	20	240	90	300	311.76	-49.8764
19	58	0	120	90	500	395.10	-51.9341
20	58	0	180	30	800	215.19	-46.6564
21	58	0	240	60	300	239.89	-47.6002
22	58	10	120	30	800	207.34	-46.7428
23	58	10	180	60	300	259.79	-48.2924
24	58	10	240	90	500	184.44	-45.3171
25	58	20	120	60	300	282.68	-49.0259
26	58	20	180	90	500	318.96	-50.0747
27	58	20	240	30	800	305.88	-49.7110

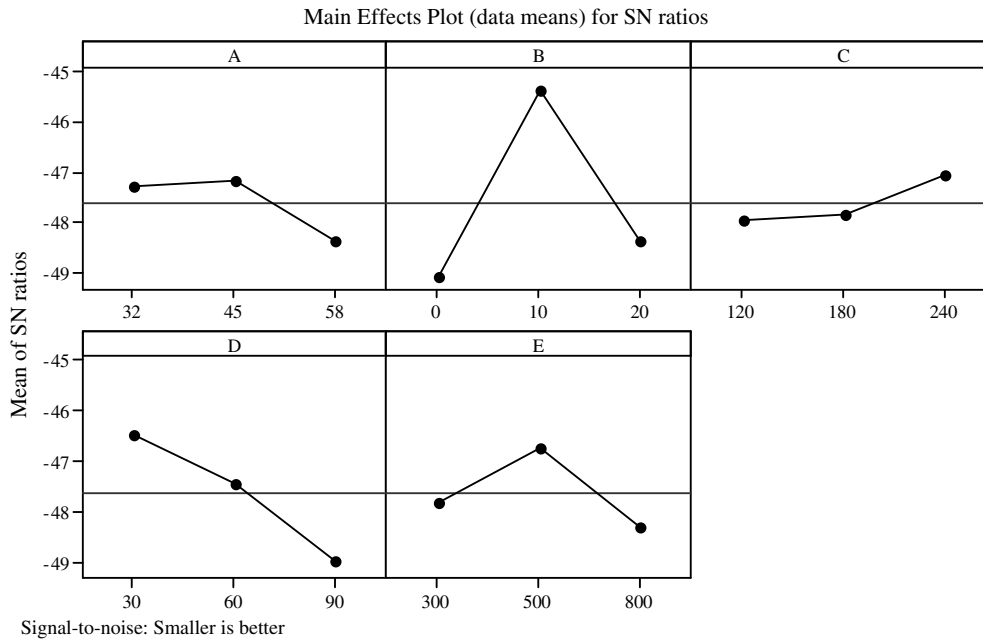


Fig. 11. Effect of control factors on erosion rate.

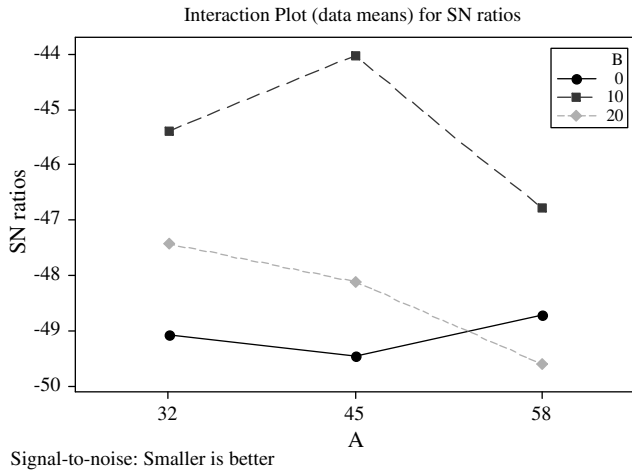


Fig. 12. Interaction graph between $A \times C$ for erosion rate.

the other hand at relatively higher impact velocity the composites exhibit ductile ($\eta < 10\%$) erosion behavior [31].

4.5. ANOVA and the effects of factors

In order to find out statistical significance of various factors like impact velocity (A), alumina percentage (B), stand-off distance (C), impingement angle (D) and erodent size (E) on erosion rate, analysis of variance (ANOVA) is performed on experimental data. Table 6 shows the results of the ANOVA with the erosion rate. This analysis is undertaken for a level of confidence of significance of 5%. The last column of the table indicates that the main effects are highly significant (all have very small p -values).

From Table 6, one can observe that alumina percentage ($p = 0.002$), impingement angle ($p = 0.025$), erodent size ($p = 0.146$) and impact velocity ($p = 0.256$) have great influence on erosion rate. The interaction of impact velocity \times alumina percentage ($p = 0.354$) shows significant contribution on the erosion rate but the remaining

factors and interactions have relatively less significant contribution on erosion rate.

5. Confirmation experiment

The optimal combination of control factors has been determined in the previous analysis. However, the final step in any design of experiment approach is to predict and verify improvements in observed values through the use of the optimal combination level of control factors. The confirmation experiment is performed by taking an arbitrary set of factor combination $A_1B_3D_2E_3$, but factor C has been omitted because factor C and interaction $A \times C$ have the least effect on erosion rate as evident from Table 6. The estimated S/N ratio for erosion rate can be calculated with the help of following prediction equation:

$$\hat{\eta}_1 = \bar{T} + (\bar{A}_1 - \bar{T}) + (\bar{B}_3 - \bar{T}) + [(\bar{A}_1\bar{B}_3 - \bar{T}) - (\bar{A}_1 - \bar{T}) - (\bar{B}_3 - \bar{T})] + (\bar{D}_2 - \bar{T}) + (\bar{E}_3 - \bar{T}) \quad (10)$$

$\hat{\eta}_1$ = Predicted average; \bar{T} = Overall experimental average; \bar{A}_1 , \bar{B}_3 , \bar{D}_2 and \bar{E}_3 = Mean response for factors and interactions at designated levels.

By combining like terms, the equation reduces to

$$\hat{\eta}_1 = \bar{A}_1\bar{B}_3 + \bar{D}_2 + \bar{E}_3 - 2\bar{T} \quad (11)$$

A new combination of factor levels A_1 , B_3 , D_1 and E_3 is used to predict deposition rate through prediction equation and it is found to be $\hat{\eta}_1 = -47.9446$ dB.

For each performance measure, an experiment is conducted for a different factors combination and compared with the result obtained from the predictive equation as shown in Table 7.

The resulting model seems to be capable of predicting erosion rate to a reasonable accuracy. An error of 4.71% for the S/N ratio of erosion rate is observed. However, the error can be further reduced if the number of measurements is increased. This validates the development of the mathematical model for predicting the measures of performance based on knowledge of the input parameters.

Table 4
Erosion efficiency for different alumina percentage

Expt. no.	Alumina percentage (%)	Impact velocity (V) m/s	Density of target material (ρ) kg/m ³	Hardness of target material (H_v) MPa	Erosion rate (E_r) mg/kg	Erosion efficiency (η)%
1	0	32	1932	39	309.83	47.91894
2	0	32	1932	39	235.25	10.49685
3	0	32	1932	39	315.19	12.18698
4	10	32	1765	38	173.77	8.26962
5	10	32	1765	38	264.94	10.92578
6	10	32	1765	38	139.96	23.08708
7	20	32	1730	36.5	289.48	11.69854
8	20	32	1730	36.5	227.49	36.77353
9	20	32	1730	36.5	197.88	9.228278
10	0	45	1932	39	318.86	7.194564
11	0	45	1932	39	349.80	6.839407
12	0	45	1932	39	235.25	18.39875
13	10	45	1765	38	174.94	3.648120
14	10	45	1765	38	133.18	11.10910
15	10	45	1765	38	172.78	4.157950
16	20	45	1730	36.5	183.96	15.03735
17	20	45	1730	36.5	287.83	6.787811
18	20	45	1730	36.5	311.76	6.371010
19	0	58	1932	39	395.10	4.650233
20	0	58	1932	39	215.19	10.13094
21	0	58	1932	39	239.89	3.258259
22	10	58	1765	38	207.34	10.41099
23	10	58	1765	38	259.79	3.763373
24	10	58	1765	38	184.44	2.315284
25	20	58	1730	36.5	282.68	4.012895
26	20	58	1730	36.5	318.96	3.923676
27	20	58	1730	36.5	305.88	15.05109

Table 5
Comparison of theoretical and experimental erosion results

Expt. no.	E_r (Theoretical) mg/kg	E_r (Experimental) mg/kg	Error (%)
1	290.42	309.83	6.68342
2	245.45	235.25	4.15563
3	314.49	315.19	0.22258
4	179.18	173.77	3.01931
5	269.46	264.94	1.67742
6	136.59	139.96	2.46724
7	288.48	289.48	0.34664
8	246.52	227.49	7.71945
9	206.34	197.88	4.10002
10	325.61	318.86	2.07303
11	356.87	349.80	1.98111
12	245.43	235.25	4.14782
13	182.16	174.94	3.96354
14	138.24	133.18	3.66030
15	186.37	172.78	7.29194
16	193.68	183.96	5.01858
17	298.47	287.83	3.56484
18	310.49	311.76	0.40903
19	407.11	395.10	2.95006
20	228.26	215.19	5.72592
21	246.19	239.89	2.55899
22	214.68	207.34	3.41904
23	276.82	259.79	6.15201
24	182.64	184.44	0.98555
25	296.46	282.68	4.64818
26	319.48	318.96	0.16276
27	307.91	305.88	0.65928

6. Factor settings for minimum erosion rate

In this study, an attempt is made to derive optimal settings of the control factors for minimization of erosion rate. The single-objective optimization requires quantitative determination of the relationship between erosion rates with combination of control factors. In order to express, erosion rate in terms of mathematical model in the following form is suggested

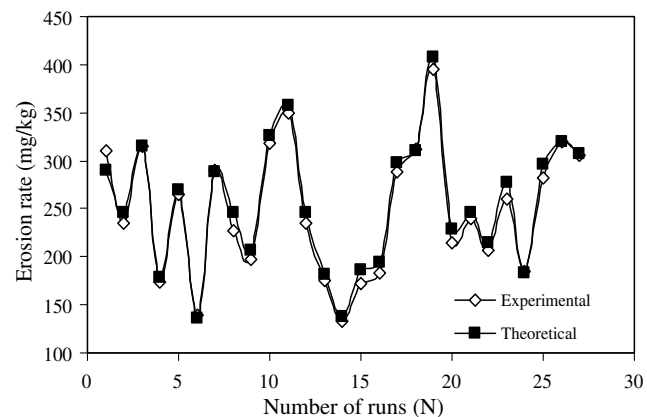


Fig. 13. Comparison plot for theoretical and experimental erosion rates.

Table 6
ANOVA table for erosion rate

Source	DF	Seq SS	Adj SS	Adj MS	F	P
A	2	7.580	7.580	3.790	1.62	0.256
B	2	68.885	68.885	34.442	14.75	0.002
C	2	4.455	4.455	2.228	0.95	0.425
D	2	28.269	28.269	14.134	6.05	0.025
E	2	11.548	11.548	5.774	2.47	0.146
A*B	4	11.968	11.968	2.992	1.28	0.354
A*C	4	5.705	5.705	1.426	0.61	0.667
Error	8	18.685	18.685	2.336		
Total	26	157.095				

$$E_r = K_0 + K_1 \times A + K_2 \times B + K_3 \times D + K_4 \times E + K_5 \times A \times B \quad (12)$$

Here, E_r is the performance output terms and K_i ($i = 0, 1, \dots, 5$) are the model constants. The constants are calculated using non-linear regression analysis with the help of SYSTAT 7 software and the following relations are obtained

Table 7
Results of the confirmation experiments for erosion rate

	Optimal control parameters	
	Prediction	Experimental
Level	$A_1B_3D_2E_3$	$A_1B_3D_2E_3$
S/N ratio for erosion rate (mg/kg)	-47.9446	-45.6864

$$Y = 0.467 - 0.031 \times A - 0.355 \times B + 0.273 \times D + 0.053 \times E + 0.382 \times A \times B$$

$$r^2 = 0.95 \quad (13)$$

The correctness of the calculated constants is confirmed as high correlation coefficients (r^2) in the tune of 0.95 are obtained for Eq. (12) and therefore, the models are quite suitable to use for further analysis. Here, the resultant objective function to be maximized is given as

$$\text{Maximize } Z = 1/f \quad (14)$$

f = normalized function for erosion rate

Subjected to constraints :

$$A_{\min} \leq A \leq A_{\max} \quad (15)$$

$$B_{\min} \leq B \leq B_{\max} \quad (16)$$

$$D_{\min} \leq D \leq D_{\max} \quad (17)$$

$$E_{\min} \leq E \leq E_{\max} \quad (18)$$

The min and max in Eqs. (15)–(18) shows the lowest and highest control factors settings (control factors) used in this study (Table 1).

Genetic algorithm (GA) is used to obtain the optimum value for single-objective outputs to optimize the single-objective function. The computational algorithm is implemented in Turbo C++ and run on an IBM Pentium IV machine. Genetic algorithms (GAs) are mathematical optimization techniques that simulate a natural evolution process. They are based on the Darwinian Theory, in which the fittest species survives and propagate while the less successful tend to disappear. Genetic algorithm mainly depends on three types of operator's viz., reproduction, crossover and mutation. Reproduction is accomplished by copying the best individuals from one generation to the next, what is often called an elitist strategy. The best solution is monotonically improving from one generation to the next. The selected parents are submitted to the crossover operator to produce one or two children. The crossover is carried out with an assigned probability, which is generally rather high. If a number randomly sampled is inferior to the probability, the crossover is performed. The genetic mutation introduces diversity in the population by an occasional random replacement of the individuals. The mutation is performed based on an assigned probability. A random number is used to determine if a new individual will be produced to substitute the one generated by crossover. The mutation procedure consists of replacing one of the decision variable values of an individual while keeping the remaining variables unchanged. The replaced variable is randomly chosen and its new value is calculated by randomly sampling within its specific range. In genetic optimization, population size, probability of crossover and mutation are set at 50, 75%, and 5%, respectively for all the cases. Number of generation is varied till the output is converted. Table 8 shows the optimum conditions of the control factors with

Table 8
Optimum conditions for performance output

Control factors and performance characteristics	Optimum conditions
A: Impact velocity (m/s)	56.89
B: Alumina percentage (%)	11.82
D: Impingement angle (degree)	61.56
E: Eroderent size (μm)	788.0
Erosion rate (mg/kg)	271.83

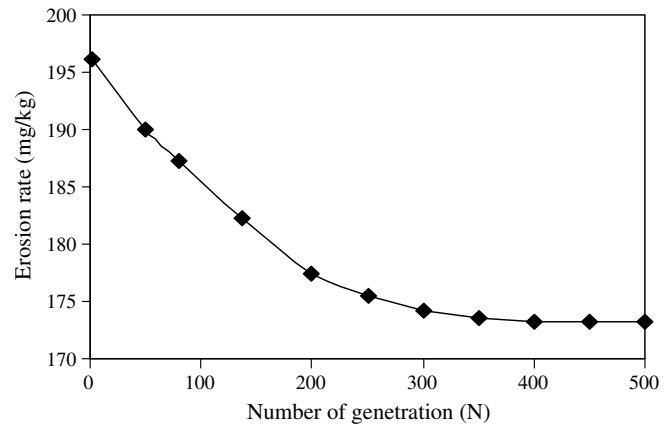


Fig. 14. Convergence curve.

optimum performance out put gives a better combination of set of input control factors. The pattern of convergence of performance output with number of generations is shown in Fig. 14.

7. Conclusions

This analytical and experimental investigation into the erosion behavior of alumina-GF-polyester hybrid composites leads to the following conclusions:

1. A mathematical model based on conservation of particle kinetic energy during multiple impact erosion process has been developed. To overcome the shortcomings of the existing theoretical models an 'erosion efficiency' term has been introduced. It is demonstrated that if supported by an appropriate magnitude of erosion efficiency, the model can perform well for polymer based hybrid composites for normal as well as oblique impacts.
2. Hybrid composites suitable for applications in highly erosive environments can be prepared by reinforcement of glass fibers and filling of micro-sized alumina particles in thermoplastic polyester resin. The erosion wear performance of these composites improves quite significantly by addition of alumina filler. On the other hand, due to the presence of these particulates, the composite suffers a loss in tensile as well as flexural strength.
3. Erosion characteristics of these composites can be successfully analyzed using Taguchi experimental design scheme. Taguchi method provides a simple, systematic and efficient methodology for the optimization of the control factors. This approach not only needs engineering judgment but also requires a rigorous mathematical model to obtain optimal process settings.
4. The erosion efficiency (η), in general, characterizes the wear mechanism of composites. The alumina filled GF-polyester composites exhibit semi-ductile erosion response ($\eta = 10\text{--}60\%$) for low impact velocities and ductile erosion response ($\eta < 10\%$) for relatively high impact velocity.
5. Factors like alumina percentage, impingement angle, erodent size and impact velocity in order of priority are significant to minimize the erosion rate. Although the effect of impact velocity is less compared to other factors, it cannot be ignored because it shows significant interaction with another factor i.e. the percentage of alumina in the composite.
6. Study of influence of impingement angle on erosion rate of the composites filled with different percentage of alumina reveals their semi-ductile nature with respect to erosion wear. The peak erosion rate is found to be occurring at 60° impingement angle under various experimental conditions.

7. The rationale behind the use of genetic algorithm lies in the fact that genetic algorithm has the capability to find the global optimal parameter settings whereas the traditional optimization techniques are normally stuck up at the local optimum values. The optimum settings are found to be impact velocity = 56.89 m/s, alumina percentage = 11.82%, impingement angle = 61.56°, erodent size = 788 µm, and resulting erosion rate = 271.83 mg/kg as far as present experimental conditions are concerned.
8. In future, this study can be extended to new hybrid composites using other potential fillers and the resulting experimental findings can be similarly analyzed.

References

- [1] Gregory Sawyer W, Freudenberg Kevin D, Bhimaraj Praveen, Schadler Linda S. A study on the friction and wear behavior of PTFE filled with alumina nanoparticles. *Wear* 2003;254:573–80.
- [2] Jung-il K, Kang PH, Nho YC. Positive temperature coefficient behavior of polymer composites having a high melting temperature. *J Appl Polym Sci* 2004;92:394–401.
- [3] Nikkeshi S, Kudo M, Masuko T. Dynamic viscoelastic properties and thermal properties of powder-epoxy resin composites. *J Appl Polym Sci* 1998;69:2593–8.
- [4] Zhu K, Schmauder S. Prediction of the failure properties of short fiber reinforced composites with metal and polymer matrix. *Comput Mater Sci* 2003;28:743–8.
- [5] Rusu M, Sofian N, Rusu D. Mechanical and thermal properties of zinc powder filled high density polyethylene composites. *Polym Test* 2001;20:409–17.
- [6] Tavman IH. Thermal and mechanical properties of copper powder filled poly (ethylene) composites. *Powder Technol* 1997;91:63–7.
- [7] Rothon RN. *Adv Polym Sci* 1999;139:67.
- [8] Rothon RN. *Adhesion* 1997;64:87.
- [9] Cirino M, Pipes RB, Friedrich K. The abrasive wear behaviour of continuous fibre polymer composites. *J Mater Sci* 1987;22:2481.
- [10] Cirino M, Friedrich K, Pipes RB. Evaluation of polymer composites for sliding and abrasive wear application. *Composites* 1988;19:383.
- [11] Lhymn C, Tempelmeyer KE, Davis PK. The abrasive wear of short fibre composites. *Composites* 1985;16:127.
- [12] Voss H, Friedrich K. On the wear behaviour of short fibre reinforced PEEK composites. *Wear* 1987;116:1.
- [13] Briscoe BJ, Yao LH, Stolarski TA. The friction and wear of PTFE and PEEK composites: an initial appraisal of the optimum composition. *Wear* 1986;108:357.
- [14] Friedrich K, Lu Z, Hager AM. Overview on polymer composites for friction and wear application. *J Theor Appl Fract Mech* 1993;19:1–11.
- [15] Bahadur S, Gong D. The role of copper compounds as fillers in the transfer and wear behaviour of PEEK. *Wear* 1992;154:151.
- [16] Wang QH, Xue QJ, Shen WC, Zhang J. The friction and wear properties of nanometer ZrO₂-filled PEEK. *J Appl Polym Sci* 1998;69:135.
- [17] Wang QH, Xue QJ, Shen WC. The tribological properties of SiC whisker reinforced PEEK. *J Appl Polym Sci* 1998;69:2341.
- [18] Wang QH, Xue QJ, Liu WM, Chen J-M. The friction and wear characteristics of nanometer SiC and PTFE filled PEEK. *Wear* 2000;243:140.
- [19] Voss H, Friedrich K. Wear performance of bulk liquid crystal polymer and its short fibre composites. *Tribol Int* 1986;19:145.
- [20] Harsha AP, Tewari US. Tribo performance of polyaryletherketone composites. *Polym Test* 2002;21:697–709.
- [21] Mishra PK. *Nonconventional machining*. New Delhi: Narosa Publishing House; 1997.
- [22] Sundararajan G, Roy M, Venkataraman B. Erosion efficiency-a new parameter to characterize the dominant erosion micromechanism. *Wear* 1990;140:369.
- [23] Stachowiak GW, Batchelor AW. *Engineering tribology*. Tribology series, vol. 24. Amsterdam: Elsevier; 1993. p. 588.
- [24] Aglan HA, Chenock Jr TA. Erosion damage features of polyimide thermoset composites. *SAMPEQ* 1993: 41–7.
- [25] Srivastava VK, Pawar AG. Solid particle erosion of glass fiber reinforced flyash filled epoxy resin composites. *Compos Sci Technol* 2006;66:3021–8.
- [26] Suresh Arjula, Harsha A P. Study of erosion efficiency of polymers and polymer composites. *Polym Test* 2006;25:188–96.
- [27] Glen SP. *Taguchi methods: a hands on approach*. New York: Addison-Wesley; 1993.
- [28] Fu S-Y, Lauke B. Characterization of tensile behavior of hybrid short glass fiber/calcite particles/ABS composites. *Composites: A* 1998;29:575–83.
- [29] Thomason JL, Vlug MA, Schipper G, Krikor HGLT. Influence of fibre length and concentration on the properties of glass fibre reinforced polypropylene: Part 3. Strength and strain at failure. *Composites A* 1996;27:1075–84.
- [30] Tewari US, Harsha AP, Hager AM, Friedrich K. Solid particle erosion of unidirectional carbon fiber reinforced polyetheretherketone composites. *Wear* 2002;252:992–1000.
- [31] Manish Roy, Vishwanathan B, Sundararajan G. The solid particle erosion of polymer matrix composites. *Wear* 1994;171:149–61.